

# EXPERIMENTAL INVESTIGATION ON HEAT TRANSFER CHARACTERISTICS OF HIGH BLOCKAGE RIBS CHANNEL

Weihua Yang.\* Shulin Xue.

\*Author for correspondence

College of Energy and Power Engineering, Nanjing University of Aeronautics and Astronautics, Nanjing, China

E-mail: Yangwh@nuaa.edu.cn

## ABSTRACT

The heat transfer and pressure loss characteristics on a square channel with two opposite surfaces roughened by high blockage ratio ribs are measured by systematic experiments. Reynolds number studied in the channel range from 1400 to 4500. The rib height( $e$ ) to hydraulic diameter( $D$ ) ratios are 0.2 and 0.33, respectively. The rib spacing( $p$ ) to height ratio( $p/e$ ) ranges from 5 to 15. The rib orientations in the opposite surfaces are symmetric and staggered arrangement. The experimental results show that (1) the heat transfer coefficients are increased with the increase of rib height and Reynolds number, though at the cost of higher pressure losses; (2) when the rib spacing to height ratio is 10, it keeps a highest heat transfer coefficient in three kinds of rib spacing to height ratio 5, 10 and 15; (3) the heat transfer coefficient of symmetric arrangement ribs is higher than the staggered arrangement ribs, but the pressure losses of symmetric arrangement ribs is larger than the staggered arrangement ribs.

## INTRODUCTION

Advanced gas turbine engines operate at high temperature to improve thermal efficiency and power output. As the turbine inlet temperature increases, the heat transferred to the turbine blades also increases. The level and variation in the temperature within the blade material must be limited to achieve reasonable durability goals. Because the operating temperature of modern gas turbines is far above the permissible metal temperature, there is a need to cool the blade for safe operation. There are two methods used for turbine blades to protect the blade material from exceeding the maximum allowable temperature, one is external cooling, such as film cooling, and another is internal cooling, such as impingement cooling, rib turbulated cooling, and pin-fin cooling. The internal cooling is achieved by passing the coolant through several enhanced serpentine passage inside the blade and extracting the heat from the outside of the blades. A common method of increasing the cooling capacity of the internal cooling circuit is the addition of rib turbulators to the internal coolant channel walls. The addition of the rib turbulators increases the overall internal convective heat transfer coefficient, causing a corresponding drop in the component metal temperature.

Over the last few decades, there have been many studies on configuration parameters such as rib shape, aspect ratio, pitch ratio, blockage ratio  $e/D_h$ , rib angle of attack, and so on [1-6]. Han and Wagner [7-11] studied the effect of Reynolds number

## NOMENCLATURE

$A$	[m <sup>2</sup> ]	heat area of stainless foil
$D$	[m]	hydraulic diameter
$h$	[W/m <sup>2</sup> K]	heat transfer coefficient
$L$	[m]	Length
$p$	[Pa]	Pressure
$Q$	[W]	heat flow of stainless foil
$T$	[K]	Temperature
$u$	[m/s]	Flow velocity

### Special characters

$\varepsilon$	[-]	Surface emissivity
$\sigma$	[m]	Stefan-Boltzmann constant
$\rho$	[kg/m <sup>3</sup> ]	Density
$\lambda$	[W/mK]	Thermal conductivity
$\nu$	[m <sup>2</sup> /s]	kinematic viscosity

### Subscripts

$a$	Air
$amb$	Ambient
$c$	Convection
$in$	Inlet
$out$	Outlet
$ow$	Outside wall
$rad$	Radiation

on the centerline heat transfer coefficient of a square channel ( $W/H=1$ ) and two rectangular channels ( $W/H=2,4$ ) for two rib spacing ( $P/e=10,20$ ). The heat transfer distribution was presented by a Nusselt number ratio with several Reynolds numbers, and they showed similar trends except that the Nusselt number ratios decreased slightly with increasing Reynolds numbers. Bailey and Han [12,13] figured out that the best rib pitch to height ratio is between 7 and 15. Han et al. [14] pointed out that the channel with angled ribs performed better than orthogonal ribs due to the stronger secondary flow. Han et al. [15,16] showed that the orthogonal ribs in the narrow channel not only induce a high heat transfer coefficient but also cause a high pressure drop. The effect of the channel aspect ratio has been studied by Han and Park [17,18]. Though the ribbed side heat transfer augmentation is of the same order in all cases, the friction factor is much higher for channels with wider aspect ratios. Studies by Taslim et al. [19] have focused on the cooling passages embedded in the leading edge of the blade. Zhang [20] experimentally studies on a ribbed triangular channel.

A flow visualization of the secondary flows is presented in Ref. [21], and a computational picture of secondary flows is painted in Ref. [22]. Su et al. [23] performed computations on a rotating channel with inclined ribs and presented predictions of

secondary flows in the first channel. Liou, et al.[24] studied the flow and heat transfer characteristics in a two-pass 90 degree ribbed parallelogram channel with infrared thermography and particle image velocimetry. It is found that the flow dynamic mechanisms responsible for the rib top and mid-rib heat transfer enhancement are different for the inlet and outlet passes. The presences of a kewed high  $Nu_0$  streak between the last inlet-leg rib and the bend as well as two high  $Nu_0$  zones inside the bend are the new found features lacking in the corresponding two-pass 90-deg ribbed square channel. In addition, simple correlations of  $Nu_0$  and  $f_0$  with  $Re$  are acquired. Thermal performance factors are about 66% and 28% higher than the previous reported smooth-walled counterpart at  $Re=5000$  and  $20,000$ , respectively. Kim[25] studied the effects of inlet velocity profile on flow and heat transfer in the entrance region of a ribbed channel. They found that in the entrance region, the location and shape of the reattachment and the recirculation region were altered by the local velocity distribution caused by the different inlet velocity profiles. Therefore, the distribution and the strength of the vorticity in the channel were changed, and the local heat transfer coefficient and pressure drop in the channel were affected by the inlet velocity profile.

From above we can know that the flow and heat transfer characteristics of rib-roughened channels has been deeply studied by a lot of researchers in the last few decades. Almost all studies in open literatures focus on higher Reynolds number (8000 at least) and a lower blockage ratio(5%~10%). However, for the smaller gas turbine, the turbine blades have higher blockage ribs and lower coolant Reynolds number at closer spacing of turbine blade. The objective of this study is to measure heat transfer coefficient and friction factor for a 90 degree parallel rib-roughened high blockage( $0.2 < e/D < 0.33$ ) square channel with pacing ( $P/e$ ) ranging from 5 to 15. The Reynolds numbers tested are between 3000 and 8000. The study results of this paper are the benefit supplement for the internal cooling design of turbine blades.

## EXPERIMENTAL SETUP

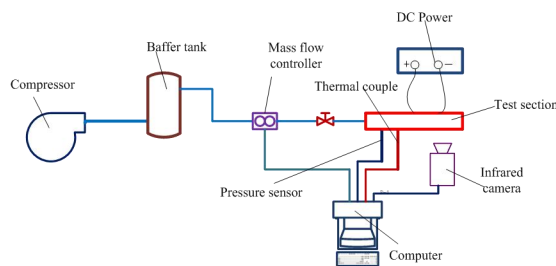


Figure.1 Experimental setup

Figure.1 shows the comprehensive scheme of experimental setup which consists of compressor, buffer tank, mass flow controller and test section. The air from compressor having environment temperature is ducted into the test section. A ball valve to protect and control the flow rate is provided upstream of the test section. The flow is measured using a mass flow controller. The temperature of the air flowing into the test section is monitored by a T-type thermocouple. The spent air

from the test section is directly exhausted into the atmosphere. The accuracy of the mass flow controller and T-type thermocouple is 1.0% and  $\pm 0.1^\circ\text{C}$ , respectively. The temperature of the test wall is measured by an infrared thermography system( TVS-2000MK) with accuracy and measured temperature range of  $\pm 0.1^\circ\text{C}$  ( $0\sim 100^\circ\text{C}$ ) for the infrared thermograph system. All the measurement data of temperature are connected with 8-channel HP34970A data collection system.

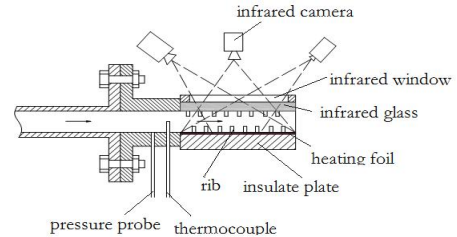


Figure 2 Schematic of test section

Figure 2 shows the schematic of the test section. There are two kinds of test section in this experiment. Both the test sections are rectangular channels. The geometrical dimensions of the test sections are  $180\text{mm}(\text{length})\times 60\text{mm}(\text{width})\times 15\text{mm}(\text{height})$  and  $180\text{mm}(\text{length})\times 60\text{mm}(\text{width})\times 9\text{mm}(\text{height})$ , respectively. At the entrance of the test section, there are a T-type thermocouple and a static pressure probe to measure the temperature and static pressure of the stream. The heating foil heated by passing DC power to provide uniform heat flux is made of  $0.02\text{mm}$  thick stainless-steel foil with  $180\text{mm}\times 60\text{mm}$  (length and width) dimensions. The surface of heating foil is painted with black paint to assure an uniform emissivity of 0.96. The channels are roughened with square cross section ribs made of stainless steel. The ribs with  $3\text{mm}\times 3\text{mm}\times 60\text{mm}$  dimensions are glued on heating foil and infrared glass, respectively. The ribs on the opposite wall are laid parallel to each other. The ribs are placed with a given spatial periodicity. The temperature of the heating foil is measured by infrared camera. In order to measure the complete temperature field of the rib roughened heating foil, it needs to measure the temperature field from three angles for the infrared camera. Three T-type thermocouples to act as reference for the infrared thermograph system are fastened on the rear of stainless steel foil with 502 glue. Eq.1 is the relationship between corrected infrared temperature and thermocouple date, respectively where  $T_0$  is the infrared thermograph temperature,  $T$  is the corrected infrared temperature.

$$T = -13.6 + 1.46T_0 - 0.00528T_0^2 \quad (1)$$

The insulated plate to minimize ambient heat transfer loss is made of a  $20\text{mm}$  thick Bakelite slab, which has a very low thermal conductivity of  $0.06 \text{ W}/(\text{m}\cdot^\circ\text{C})$ . Three T-type thermocouples are glued on the outside of the insulated plate.

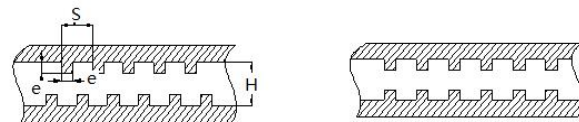


Fig.3a Staggered arrangement Fig.3b Symmetric arrangement

Figure 3 Schematic of rib arrangement

There are two kinds of rib arrangement for the rib roughened channel, one is symmetric arrangement, another is staggered arrangement. The geometry dimensions of rib roughened channel are shown in Figure.3 and Table 1.

Tab.1 Geometry dimensions of rib roughened channel

Rib arrangement	$e$	$H$	$P$	$P/e$	$e/D$
Symmetric arrangement	3	15	15	5	0.2
			30	10	
			45	15	
	3	9	15	5	0.33
			30	10	
			45	15	
Staggered arrangement	3	15	15	5	0.2
			30	10	
			45	15	
	3	9	15	5	0.33
			30	10	
			45	15	

## DATA REDUCTION

The Reynolds number is computed using the expression

$$Re = \frac{uD}{\nu} \quad (2)$$

where  $u$  is the velocity in the test section, which is computed from the mass flow rate calculated from the mass flow controller.  $D$  is the hydraulic diameter of the test section,  $\nu$  is the kinematic viscosity.

The heat transfer coefficient,  $h$  is estimated as

$$h = \frac{Q - Q_{loss}}{A(T_w - T_a)} \quad (3)$$

where,  $Q = UI$  is the heat flow of stainless foil when the foil is being heated by passing DC power which has the accuracy of  $\pm 0.1V$  and  $\pm 0.1A$  for voltage  $U$  and electric current  $I$ , respectively.  $A$  is the heat area of stainless foil. As the desired voltage  $V$  and current  $I$  passing through the test plate, the heat flux  $Q$  along the surface of stainless foil can be calculated.  $T_w$  is the wall temperature of stainless foil heated by passing DC power. The  $T_a$  is the air temperature at the inlet section of the test section which can be measured by the T-type thermocouple.

$Q_{loss} = Q_{con} + Q_{rad}$  is the heat loss from the outer surface of the insulated plate to ambient, which includes natural convection heat loss  $Q_{con}$  and radiation heat loss  $Q_{rad}$ . The natural convection heat loss  $Q_{con}$  is calculated by:

$$Q_{con} = Ah_{nat}(T_{ow} - T_{amb}) \quad (4)$$

where  $h_{nat}$  is the natural convection heat transfer coefficient which can be obtained by[26]:

$$Nu_{nat} = 0.59(Gr Pr)^{0.25} \quad (5)$$

$T_{ow}$  is the outer surface temperature of the insulated plate,  $T_{amb}$  is the ambient temperature.  $Gr$  and  $Pr$  are the Grashof number and Prandtl number, respectively.

The radiation heat loss  $Q_{rad}$  is calculated by

$$Q_{loss} = \sigma \varepsilon A(T_w^4 - T_{amb}^4) \quad (6)$$

where  $\sigma = 5.67 \times 10^{-8} W/(m^2 K^4)$  is the Stefan-Boltzmann constant,  $\varepsilon_{ow} = 0.6$  is the outer surface emissivity of the insulated plate.

The temperature distribution on the surface of stainless foil(heated or unheated) was recorded by an infrared thermography system operating in the middle IR band(8-14 $\mu m$ ) of the infrared spectrum. The temperature calculation method of the temperature map obtained from the infrared thermography system was described in Ref.[27]. During all of the experiments, the outer surface temperature of the insulated plate is between 25.5°C and 25°C while ambient temperature is approximately 24°C. The difference between ambient temperature and outer surface temperature of the insulated plate is less than 1.5°C. So, the natural convection heat loss is about 0.1W, the radiation heat loss is about 0.145W, the total heat loss  $Q_{loss}$  is about 0.245W which is far less than the heat flow  $Q$ . Thus, it is reasonable to ignore the heat loss from the outer surface of the insulated plate.

The average Nusselt number is defined as

$$Nu = \frac{hD}{\lambda} \quad (7)$$

where  $\lambda$  is the thermal conductivity of the air.

The friction factor is defined as

$$f = \frac{1}{2} \frac{D}{\rho u^2} \frac{p_{in} - p_{out}}{\Delta L} \quad (8)$$

where  $p_{in}$  and  $p_{out}$  are the pressure of the inlet section and outlet section of the test section. The average inlet velocity  $u$  is calculated using the channel mass flow rate.  $\Delta L$  is the length of the test section.

The smooth channel correlations of Dittus–Boelter and Moody are utilized for normalizing the ribbed channel data, as is conventional in literature. The classical Dittus–Boelter correlation is

$$Nu_0 = 0.023 Re_f^{0.8} Pr_f^{0.4} \quad (9)$$

According to Holman[28], experimental uncertainties in average Nusselt number, friction factor measurement were estimated to be about  $\pm 9.5\%$  and  $\pm 6.3\%$ , respectively. The individual uncertainty in air stream temperature  $T_a$  was  $\pm 0.4^\circ C$ ; heating foil temperature  $T_w$  was  $\pm 0.1^\circ C$ .

## Results and analysis

Figure.4 shows the effect of rib spacing on Nusselt number for staggered and symmetrical rib channels. It can be seen that the rib pitch-to-height ratio has a large effect on the heat transfer coefficient of rib roughened channel. The rib pitch-to-height ratio equal to 10 corresponds to the largest heat transfer coefficient whether the rib arrangement is symmetrical or staggered. Clearly, the rib pitch-to-height ratio equal to 15 corresponds to the smallest heat transfer coefficient for symmetrical rib channel and staggered rib channel. The heat transfer coefficient of rib pitch-to-height ratio equal to 5 is between  $S/e=10$  and 15. This indicates that, for the ribbed channels with larger blockage ratios(0.33,0.2), the effect of rib spacing on heat transfer coefficient is not in a monotony increasing trend with the increase of rib spacing but an optimum rib pitch to height ratio. The optimum pitch to height ratio in this experiment is 10. This conclusion is the same as the Ref.[12,13]. At the same time, it also can be seen clearly that

the heat transfer coefficient linearly increases with the increase of Reynolds number. In general, the main reasons to enhance convective heat transfer in rib roughened channel are the flow separation vortex behind ribs and the reattachment to the channel wall(Fig.5). However, as the increase of the rib pitch, the effects of separation vortex and reattachment on the convective heat transfer are weaker and weaker, but the effect flowing over a flat region after the reattachment region on convective heat transfer is increased gradually. When rib spacing is large enough( $S/e=15$ ), the convective heat transfer of flow over flat is the main reason influencing on the convective heat transfer in the ribbed channel, resulting in a lower convective heat transfer coefficient. On the other hand, the flow reattachment to the rib wall will be gradually weakened as the decrease of rib pitch. When the rib pitch is small enough( $S/e=5$ ), the phenomena of flow reattachment will be disappeared, which also results in a lower heat transfer coefficient in the rib roughened channel. Thus, only when the rib spacing is appropriate( $S/e=10$ ) in ribbed channel, both of the flow separation vortex and reattachment to rib wall can play main roles on the convective heat transfer, leading to an optimum convective heat in the rib roughened channel.

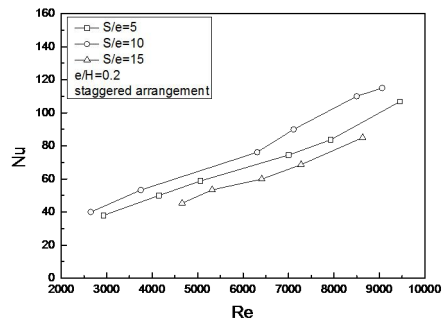


Fig.4d

Figure 4 Effect of rib pitch-to-height ratio  $P/e$  on Nusselt number

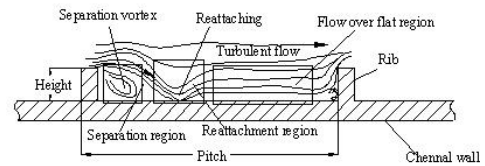


Figure 5 Schematic flow field of rib roughened channel

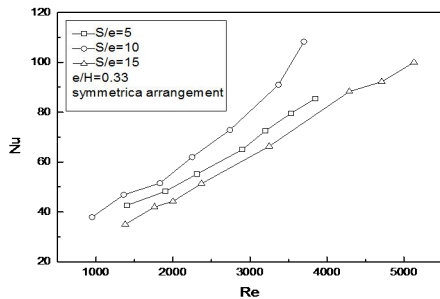


Fig.4a

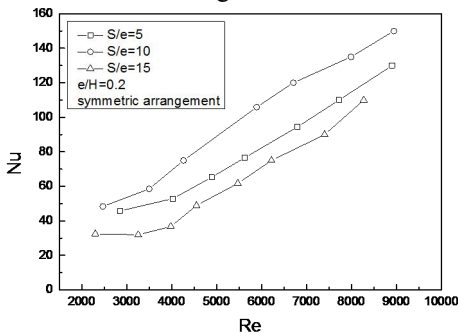


Fig.4b

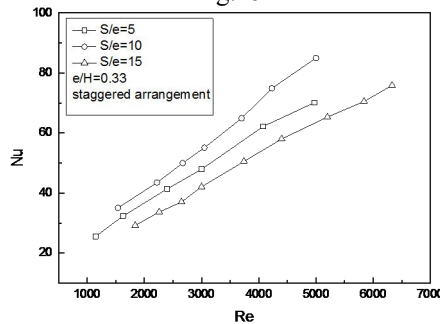


Fig.4c

Figure.6 shows the effect of rib arrangement on the heat transfer coefficient for the blockage ratio  $e/H=0.33$  and  $0.2$ . The plotted results show that rib arrangement has a larger effect on the heat transfer coefficient of rib-roughened channel. In general, the average Nusselt number of symmetric ribs is higher than that of staggered ribs. However, the difference of Nusselt number between symmetric ribs and staggered ribs is different for different blockage ratio  $e/H$ . It is increased with increasing the blockage ratio  $e/H$ . The difference of Nusselt number for  $e/H=0.33$  is larger than that for  $e/H=0.2$ .

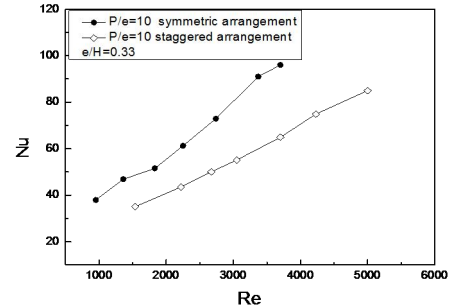


Fig.6a

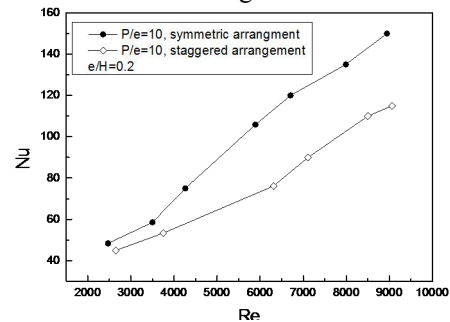


Fig.6b

Figure 6 Effect of rib arrangement on Nu

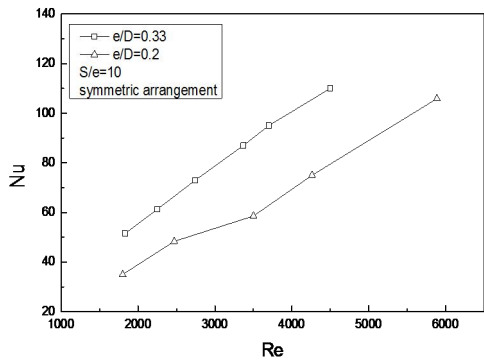


Fig.7a symmetrical arrangement

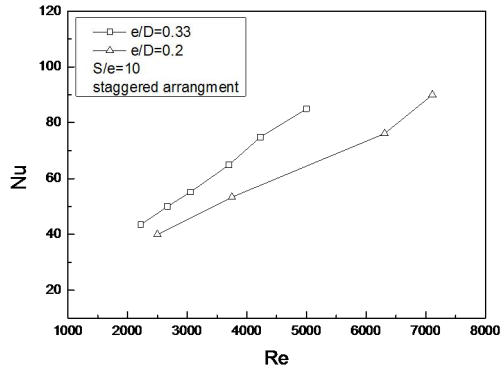


Fig.7b staggered arrangement

Figure 7 Effect of blockage ratio on heat transfer coefficient

Figure.7 shows the effect of rib blockage ratio on heat transfer coefficient. It can be seen that there is a large effect for the blockage ratio on the heat transfer coefficient. In general, a larger blockage ratio in the ribbed channel corresponds to a higher heat transfer coefficient. So, the heat transfer coefficient of blockage ratio  $e/H=0.33$  is higher than that of blockage ratio  $e/H=0.2$ . However, because of the difference of rib arrangements, the difference of heat transfer coefficient between the two blockage ratios is also different. Clearly, the difference of heat transfer coefficient for the symmetrical rib arrangement is higher than that for the staggered rib arrangement. The reason to explain this kind of phenomena is that whether symmetrical rib channel or staggered rib channel, the flow disturbance in the rib channel with  $e/H=0.33$  is significantly higher than that in the rib channel with  $e/H=0.2$ , which results in a larger heat transfer coefficient for the rib channel with  $e/H=0.3$ .

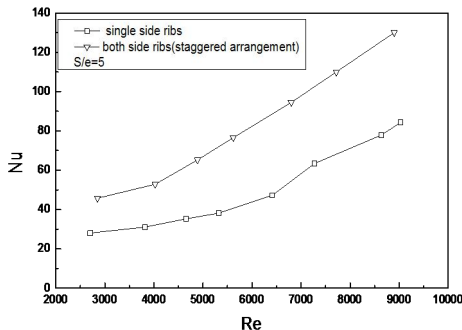


Fig.8a

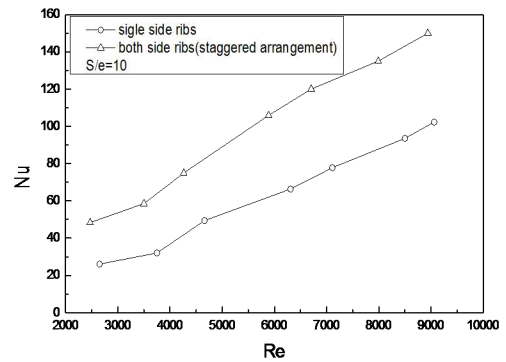


Fig.8c

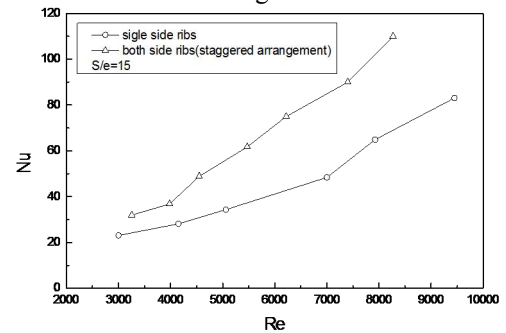


Fig.8c

Figure 8 Comparison of heat transfer coefficient between two sides rib channel and one side rib channel

Fig.8 shows the comparison of heat transfer coefficient between one-side rib channel and two-side rib channel. Clearly, the heat transfer coefficient of two-side rib channel is distinct higher than that of one-side rib channel. The difference is increased with increasing flow Reynolds number, which is from the smallest value 10 at the  $Re=3000$  up to the largest value 60 at the  $Re=9000$ . The reason for this phenomena is that both of the flow separation vortices and reattachment to the heat wall in the one-side rib channel are distinct weaker than that in two-side rib channel, thus the disturbance in the one-side rib channel is far less than that in the two-side rib channel, which results in a weaker turbulent mixing in one-side rib channel than that in two-side rib channel. So, the heat transfer coefficient of two-side ribbed channel is distinct larger than that of one-side ribbed channel.

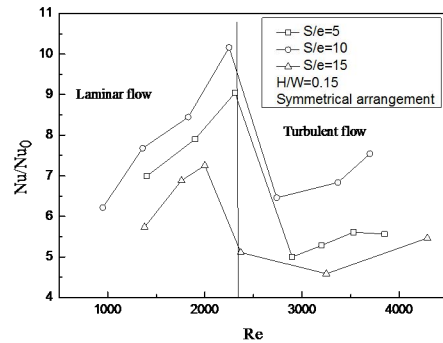


Fig.9a Symmetrical arrangement

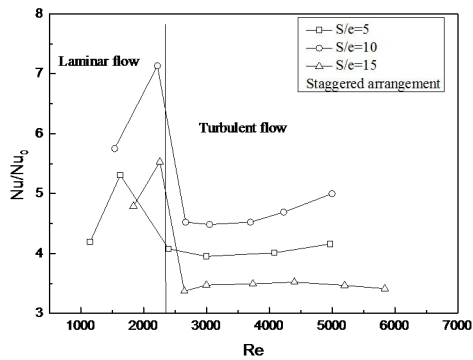


Fig.9b Staggered arrangement

**Figure 9** Average Nusselt number ratio as a function of Reynolds number( $H/W=0.15$ )

Fig.9 shows the average Nusselt number ratio  $Nu/Nu_0$  for all different ribbed channels as a function of the Reynolds number.  $Nu_0$  is the Nusselt number of smooth channel. In general, when the fluid flows through smooth tube, if the flow Reynolds number  $Re < 2300$ , the flow is laminar flow, if the  $Re > 2300$ , the flow is turbulent flow. Thus, when the flow Reynolds number  $Re < 2300$ , the average Nusselt number  $Nu_0$  for fully developed laminar flow in duct is 6.1[29]; when the  $Re > 2300$ , the  $Nu_0$  can be obtained by the equation (9). So, the average Nusselt number ratio curves are divided two regions, one is laminar region, the other is turbulent region. It can be observed that there exists a large difference for the heat transfer enhancement in the two regions. In the laminar region, the heat transfer enhancement rapidly increases with increasing Reynolds number. For the symmetrical rib channel, as the increase of the Reynolds numbers from 1000, 1400, and 1300 to 2250,2300 and 2000, the heat transfer enhancements are about 6-10 times, 7-9 times and 5.5-7 times for the ribbed channel with  $S/e=10,15$ , and 5, respectively, compared with the smooth duct. For the staggered rib roughened channel, as the increase of the Reynolds numbers from 1500, 1000, and 1700 to 2100,1500 and 2200, the heat transfer enhancements are about 5.8-7.2 times, 4.2-5.4 times and 4.8-5.5 times for the ribbed channel with  $S/e=10,15$ , and 5, respectively. However, the increase of the heat transfer enhancements with increasing Reynolds number from 3000 to 6000 in the turbulent region is far less than that in the laminar region, the largest heat transfer enhancements are about 6.5-7.5 times and 4.5-5times for symmetrical and staggered rib channels with  $S/e=10$ , respectively. Especially for the ribbed channel with  $S/e=15$ , there is almost no any change for the heat transfer enhancement with the increase of Reynolds number. This indicates that the heat transfer enhancement effectiveness of ribbed channel in the laminar flow state is far higher than that in the turbulent state.

Since the heat transfer enhancement in ribbed channel is typically accompanied by an increase in pressure drop, a comprehensive analysis of performance must include the effect of ribs on channel pressure drop. Fanning friction factor of the ribbed channels can be calculated according to Eq.(8). Fig.10 shows the experimental results for the friction factor in different ribbed channels. The friction factor, deduced from the experimental data, is depicted as a function of  $Re$ . It can be

discovered that the friction factor curves versus Reynolds number are similar to parabolas. When the  $Re < 2500$ , the friction factor  $f$  is almost linearly decreased with the increase of Reynolds number, which is similar to traditional laminar flow in tube. When the Reynolds number increases to 2000-3000, the friction factor reaches the minimum value, and then, the friction factor will increase with increasing Reynolds number, which is the same as the traditional turbulent flow in tube. Such a phenomenon indicates that when the fluid flows in rib roughened channel with large blockage ratio( $e/H=0.2,0.33$ ), the transition from laminar to turbulent flow will occur when the Reynolds number is in the range of 2000-3000, which is the same as the traditional transition Reynolds number range in smooth tube. At the same time, the ribbed channel with  $S/e=10$  corresponds to the largest friction factor. The smallest friction factor corresponds to the ribbed channel with  $S/e=15$ . It clearly presents that the optimum heat transfer coefficient corresponds to the largest friction factor, and the minimum heat transfer coefficient corresponds to the smallest friction factor.

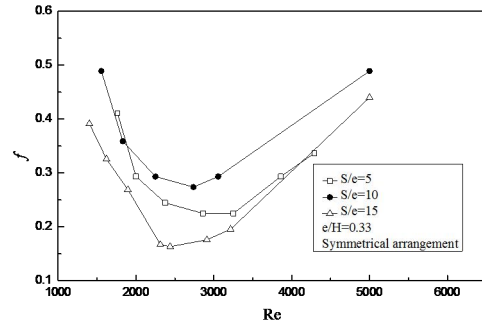


Fig.10a

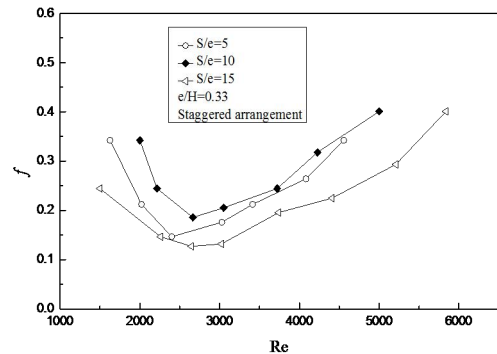


Fig.10b

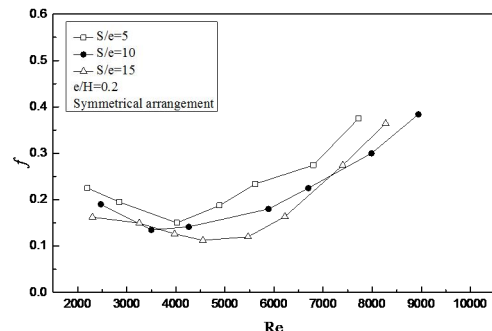


Fig.10c

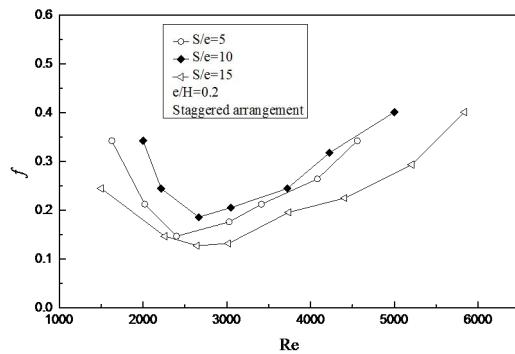


Fig.10d

Figure 10 Friction factor versus Reynolds number

## CONCLUSIONS

Heat transfer characteristics and pressure drop in rectangular rib roughened channels have been experimentally investigated by means of infrared thermography. Based on the results, the following conclusions are drawn:

(1) The rib pitch to height has a large effect on the heat transfer of the ribbed channel. The effect of rib pitch to height ratio on heat transfer coefficient is not in a monotony increasing trend but an optimum rib pitch to height ratio. The optimum pitch to height ratio in this experiment is 10.

(2) The rib arrangement has a larger effect on the heat transfer coefficient of rib-roughened channel. In general, the average Nusselt number of symmetric ribs is higher than that of staggered ribs.

(3) A larger blockage ratio in the rib roughened channel corresponds to a larger heat transfer coefficient. The heat transfer coefficient of blockage ratio  $e/H=0.33$  is larger than that of blockage ratio  $e/H=0.2$ . The heat transfer coefficient of two-side rib channel is larger than that of one-side rib channel.

(4) The heat transfer enhancement effectiveness of ribbed channel in the laminar flow state is far higher than that in the turbulent state. The optimum heat transfer coefficient corresponds to the largest friction factor, and the minimum heat transfer coefficient corresponds to the smallest friction factor.

## Acknowledgments

This work was supported by the Research Program of the National Natural Science Foundation of China, No. 51276088.

## REFERENCES

- [1] Liou, T., and Hwang, J., Effect of ridge shapes on turbulent heat transfer and friction in a rectangular channel, *Int. J. Heat Mass Transfer*, Vol.36, 1993, pp. 931–940.
- [2] Han, J. C., Glicksman, L. R., and Rohsenow, W. M., An investigation of heat transfer and friction for rib-roughened surfaces, *Int. J. Heat Mass Transfer*, Vol.2, 1978, pp.1143–1156.
- [3] Taslim, M. E., Li, T., and Kercher, D. M., Experimental heat transfer and friction in channels roughened with angled, v-shaped, and discrete ribs on two opposite walls, *ASME J. Turbomach.*, Vol.118, 1996, pp.20–28.
- [4] Kim, K. M., Lee, H., and Kim, B. S., Optimal design of angled rib turbulators in a cooling channel, *Int. J. Heat Mass Transfer*, Vol.45, 2009, pp.1617–1625.
- [5] Astarita, T., and Cardone, G., Convective heat transfer in a square channel with angled ribs on two opposite walls, *Exp. Fluids*, Vol.34, 2003, pp.625–634.
- [6] Taslim, M. E., and Liu, H. A, A combined numerical and experimental study of heat transfer in a roughened square channel with 45-deg ribs, *Int. J. Rotating Mach.*, Vol.1, 2005, pp. 60–66.
- [7] Han J. C. Heat transfer and friction characteristics in rectangular channels with rib turbulators. *ASME J. of Heat Transfer*. Vol.110, 1988,pp.321-328
- [8] Han, J. C., Dutta, S., and Ekkad, S. V., *Gas Turbine Heat Transfer and Cooling Technology*, Taylor & Francis, New York, 2000.
- [9] Wagner, J. H., Johnson, B. V., and Hajek, T. J., Heat transfer in rotating passages with smooth walls and radial outward flow, *ASME J. Turbomach.*, Vol.113, 1991, pp. 42–51.
- [10] Wagner, J. H., Johnson, B. V., and Kooper, F. C., heat transfer in rotating passage with smooth walls,” *ASME J. Turbomach.*, Vol.113, 1991, pp.321–330.
- [11] Han, J. C., Zhang, Y. M., and Kalkuehler, K., Uneven wall temperature effect on local heat transfer in a rotating two-pass square channel with smooth walls, *ASME J. Heat Transfer*, Vol.115, 1993, pp. 912–920.
- [12] J.C. Bailey, R.S. Bunker, Heat transfer and friction with very high blockage 45 deg staggered turbulators, *ASME Paper No. GT2003-38611*, 2003.
- [13] J.C. Han, Heat transfer and friction in channels with two opposite rib roughened walls, *ASME J. Heat Transfer*, Vol. 106,1984, pp. 774–781.
- [14] J.C. Han, Heat transfer and friction characteristics in rectangular channels with rib turbulators, *ASME J. Heat Transfer*, Vol.110, 1988, pp. 321–328.
- [15] J.C. Han, S. Dutta, Internal convection heat transfer and cooling: an experimental approach, Lecture Series 1995–05 on Heat Transfer and Cooling in the Gas turbines, von Karman Institute for Fluid Dynamics, Belgium, Europe, 1988. May 8–12.
- [16] J.C. Han, J.S. Park, Developing heat transfer in rectangular channels with rib turbulators, *Int. J. Heat Mass Transfer*, Vol.31, 1988, pp.183–195.
- [17] Han, J. C., and Park, J. S., Developing heat transfer in rectangular channels with rib turbulators, *Int. J. Heat Mass Transfer*, Vol.31, 1988, pp. 183–195.
- [18] Park, J. S., Han, J. C., Ou, S., and Boyle, R. J., Heat transfer performance comparisons of five different rectangular channels with parallel angled ribs, *Int. J. Heat Mass Transfer*, Vol.35, 1992, pp. 2891–2903.
- [19] Taslim, M. E., Li, T., and Spring, S. D., Measurements of heat transfer coefficients and friction factors in rib roughened channels simulating leading edge cavities of a modern turbine blade, *ASME J. Turbomach.*, Vol.119, 1997, pp. 601–609.

- [20] Zhang, Y. M., Gu, W. Z., and Han, J. C., Augmented heat transfer in triangular ducts with full and partial ribbed walls, *J. Thermophys. Heat Transfer*, Vol.8, 1994, pp. 574–579.
- [21] Kiml, R., Mochizuki, S., and Murata, A., Effects of rib arrangements on heat transfer and flow behavior in a rectangular rib-roughened passage: application to cooling of gas turbine blade trailing edge, *ASME J. Heat Transfer*, Vol.123, 2001, pp. 675–681.
- [22] Stephens, M. A., Chyu, M. K., Shih, T. P., and Cirinskas, K. C., Calculations and measurements of heat transfer in a Square Duct With Inclined Ribs, *Proceedings of the Joint propulsion conference and exhibit*, Lake Buena Vista, FL, 1996, Jul. 1–3.
- [23] Su, G., Chen, H. C., Han, J. C., and Heidman, J. D., Computation of flow and heat transfer in two-pass rotating rectangular channels (AR =1:1, AR=1:2, AR=1:4) with 45-deg angled ribs by a reynolds stress turbulence model, *ASME Paper No. GT2004-53662*.
- [24] T.M. Liou, S.W. Chang, C.Y. Huang, S.P. Chan, Y.A. Lan, Particle image velocimetry and infrared thermography measurements in a two-pass 90-deg ribbed parallelogram channel, *Int. J. of Heat and Mass Transfer*, Vol. 93, 2016, pp. 1175–1189
- [25] Dae Hyun Kim, Byung Ju Lee, Jung Shin Park, Jae Su Kwak, Jin Taek Chung, Effects of inlet velocity profile on flow and heat transfer in the entrance region of a ribbed channel, *Int. J. of Heat and Mass Transfer*, Vol. 92, 2016, pp.838–849
- [26] Yang Shiming, Tao Wenquan. Heat transfer. *Higher Education Press*, China, 2006.
- [27] Weihua Yang, Xue Liu, Guohui Li, Jingzhou Zhang, Experimental investigation on heat transfer characteristics of film cooling using parallel-inlet holes, *Int. J. of Thermal Sciences*. Vol.60, 2012, pp.32-40
- [28] J.P. Holman, *Experimental Methods for Engineerings*, 4th ed., McGraw\_hill, New York, 1984
- [29] J.P. Holman. Heat transfer. China Machine Press. 2005.